Quantum Simulation with Hybrid Tensor Networks

Xiao Yuan,[1,2,*] Jinzhao Sun,[3,†] Junyu Liu,[4,5,‡] Qi Zhao,[6,§] and You Zhou[7,‖]

[1]Center on Frontiers of Computing Studies, Department of Computer Science, Peking University, Beijing 100871, China
[2]Stanford Institute for Theoretical Physics, Stanford University, Stanford, California 94305, USA
[3]Clarendon Laboratory, University of Oxford, Parks Road, Oxford OX1 3PU, United Kingdom
[4]Walter Burke Institute for Theoretical Physics, California Institute of Technology, Pasadena, California 91125, USA
[5]Institute for Quantum Information and Matter, California Institute of Technology, Pasadena, California 91125, USA
[6]Joint Center for Quantum Information and Computer Science, University of Maryland, College Park, Maryland 20742, USA
[7]Department of Physics, Harvard University, Cambridge, Massachusetts 02138, USA

(Received 2 November 2020; revised 28 April 2021; accepted 14 June 2021; published 20 July 2021)

Tensor network theory and quantum simulation are, respectively, the key classical and quantum computing methods in understanding quantum many-body physics. Here, we introduce the framework of hybrid tensor networks with building blocks consisting of measurable quantum states and classically contractable tensors, inheriting both their distinct features in efficient representation of many-body wave functions. With the example of hybrid tree tensor networks, we demonstrate efficient quantum simulation using a quantum computer whose size is significantly smaller than the one of the target system. We numerically benchmark our method for finding the ground state of 1D and 2D spin systems of up to 8×8 and 9×8 qubits with operations only acting on $8 + 1$ and $9 + 1$ qubits, respectively. Our approach sheds light on simulation of large practical problems with intermediate-scale quantum computers, with potential applications in chemistry, quantum many-body physics, quantum field theory, and quantum gravity thought experiments.

DOI: 10.1103/PhysRevLett.127.040501

A major challenge in studying quantum many-body physics stems from the hardness of efficient representation of quantum wave functions. The tensor network (TN) theory, originated from the density matrix renormalization group for 1D Hamiltonians [1,2], provides a potential solution by describing the state with a network consisting of low-rank tensors [3]. Despite its notable success in various problems, the TN theory is inadequate to represent arbitrary systems, such as those behaving volume-law of entanglement. This motivates an alternative approach of quantum simulation, which uses a controlled quantum hardware to represent the target quantum system naturally [4]. Quantum simulation can be used for studying complex many-body systems, such as quantum chemistry and the Hubbard model [5,6]. While conventional quantum simulation algorithms require universal quantum computing, which is challenging to current technology [7], whether near-term quantum devices [8] are capable of solving realistic problems remains open [9–15]. Major technological challenges include whether we can control a sufficient number of qubits and whether the gate fidelity is sufficiently low to guarantee the calculation accuracy.

Here, we propose a hybrid TN approach to address these challenges. Leveraging the ability of TNs and quantum computers in efficient classical and quantum representation of quantum states, we introduce a framework of hybrid TN, which enables simulation of large systems using a small quantum processor with a shallow circuit. Previous studies along this line include chemistry computation beyond the active-space approximation [16], concatenation of quantum states to a matrix product state (MPS) [17], etc. Our result unifies these existing task-tailored schemes; yet, more importantly, it provides the basis for general hybrid classical-quantum representation of many-body wave functions that is applicable to broad problems. We show this by considering an example of hybrid tree TNs (TTNs) and demonstrating its application in studying static and dynamic problems of quantum systems [18,19]. We numerically test our method in finding ground states of 1D spin clusters and 2D spin lattices with up to 8×8 and 9×8 qubits.

Framework.—We first introduce the framework of hybrid tensor networks. We focus on qubits, and the results can be straightforwardly generalized to higher dimensions. A rank-n tensor, when regarded as a multi-dimension array, can be represented as $T_{j_1,j_2,\ldots,j_n}$ with n indices. The amplitude of an n-partite quantum state in the computational basis corresponds to a rank-n tensor $|\psi\rangle = \sum_{j_1,j_2,\ldots,j_n} \psi_{j_1,j_2,\ldots,j_n} |j_1\rangle|j_2\rangle\ldots|j_n\rangle$. A classical TN consists of low-rank tensors, see Fig. 1(a), which can efficiently describe physical states that lie in a small subset of the whole Hilbert space. For example, a MPS [20] $|\psi\rangle = \sum_{j_1\cdots j_n} \mathrm{Tr}[A^{j_1}\ldots A^{j_n}]|j_1\ldots j_n\rangle$ consists of rank-3 tensors with a small bond dimension κ of each matrix A^{j_k}, and

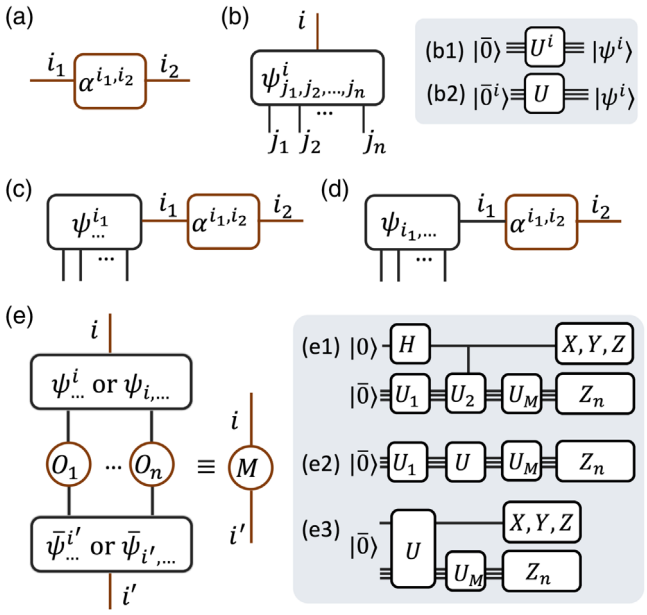

FIG. 1. Hybrid tensors and tensor contraction. (a) A low-rank classical tensor. (b) An $n+1$ rank tensor with n indices representing an n-partite quantum system and 1 classical index. Each state could be prepared with (b1) different unitary as $|\psi^i\rangle = U^i|\bar{0}\rangle$ or (b2) different initial states as $|\psi^i\rangle = U|\bar{0}^i\rangle$. (c),(d) Tensor contraction between a quantum and a classical tensor. The contracted index could be (c) classical or (d) quantum, which shares the same mathematical definition, but is contracted in different ways. (e) Expectation values of local observables for a rank-$(n+1)$ tensor as a Hermitian observable $M^{i',i} = \langle\psi^{i'}|O_1 \otimes O_2 \otimes \cdots \otimes O_n|\psi^i\rangle$. (e1) Suppose the index i is classical and $|\psi^i\rangle = U^i|\bar{0}\rangle$, we get each $M^{i',i}$ by measuring the ancillary qubit in the three Pauli bases and the other n qubits in the Z basis, with $U_1 = U^i$, $U_2 = U^{i'}(U^i)^\dagger$, and U_M being the unitary that rotates to the observable basis. (e2) Suppose the index i is classical and $|\psi^i\rangle = U|\bar{0}^i\rangle$, we use U_1 to prepare four input states $|\bar{0}^i\rangle, |\bar{0}^{i'}\rangle, (|\bar{0}^i\rangle + |\bar{0}^{i'}\rangle)/\sqrt{2}, (|\bar{0}^i\rangle + i|\bar{0}^{i'}\rangle)/\sqrt{2}$, and each $M^{i',i}$ corresponds to a linear combination of the measurement results. (e3) Suppose the index i is quantum, after applying the unitary U for preparing the state $|\psi\rangle = U|\bar{0}\rangle$; we measure n qubits in the Z basis and the other qubit in the Pauli X, Y, and Z bases.

compresses the state dimension from $O(2^n)$ to $O(n\kappa^2)$. A quantum computer prepares states $|\psi\rangle$ by applying a unitary circuit to some initial states. We can further add a classical index to the n-qubit state to form a rank-$(n+1)$ tensor $\{|\psi^i\rangle\}$; see Fig. 1(b).

Regarding low-rank tensors as classical tensors (superscript index) and quantum states as quantum tensors (subscript index), we define hybrid TNs as networks constructed by connecting both classical and quantum tensors. For example, the tensor A^{i_1,i_2} represents a classical tensor with two classical indices and $\psi^i_{j_1,j_2,\ldots,j_n}$ represents a set of n-partite quantum states. Two tensors, being either classical or quantum, are connected by following the conventional contraction rule, such as $C^{i_1,i_3} = \sum_{i_2} A^{i_1,i_2}B^{i_2,i_3}$. For example, we show the connections of a quantum and a classical tensor in Figs. 1(c) and 1(d) and refer to Ref. [21] for general cases.

While the mathematical rules are the same, classical and quantum tensors are contracted in two different ways via tensor contraction and quantum state measurement, respectively. For a rank-$(n+1)$ quantum tensor, we show how to calculate expectation values of local observables in Fig. 1(e). Calculating expectation values of general hybrid TNs works similarly, although the complexity highly depends on the network and the contraction order (see Ref. [21] for details).

Hybrid tree TN.—Contracting a general-structured TN may have exponential complexity, explaining why conventional TN theories consider networks with specific topology, including 1D MPS [22–24], 2D projected entangled pair states (PEPS, approximate contraction) [25], tree TNs [26], multiscale entanglement renormalization ansatz [27], etc. Here we consider hybrid TNs with a tree structure such as in Fig. 2(a), which admits an efficient tensor contraction. Each node is either a quantum tensor or any efficiently contractable classical TN.

We consider several tree structures with depth 2. By connecting a classical tensor to a quantum tensor, we extend the state subspace as in Fig. 2(b) or represent virtual qubits as in Fig. 2(c). Specifically, denoting the classical tensor as α^i, the network in Fig. 2(b) describes a subspace $\{|\psi\rangle = \sum_i \alpha^i|\psi^i\rangle\}$, which, when applied in quantum simulation, is a generalization of the subspace expansion method that has been widely used for finding excited energy spectra [28], error mitigation [29], and error correction [30]. For the network in Fig. 2(c), it describes the scenario where we use a quantum state and a classical tensor to, respectively, represent the active and virtual space or multidegrees of freedom, as in quantum chemistry and condensed matter [16,31–33]. We can further connect two quantum tensors via a classical tensor as in Fig. 2(d), representing weakly interacted two subsystems as considered in Ref. [17].

Its generalization to multiple subsystems is given in Fig. 2(e), where entanglement of local subsystems is described by quantum states while the correlation between local subsystems is described classically. Such a hybrid TN can be useful for describing weakly coupled subsystems, such as clustered systems. We can also use classical tensors to represent local correlations while we can use a quantum tensor to represent the nonlocal correlation, as shown in Fig. 2(f), which may be useful for studying topological order with long-range entanglement [34,35]. The construction of tree networks can be understood as an effective renormalization procedure, and other classical TNs such as the multiscale entanglement renormalization ansatz can be similarly used [21]. In addition to representing either local correlations or nonlocal correlations with classical tensors,

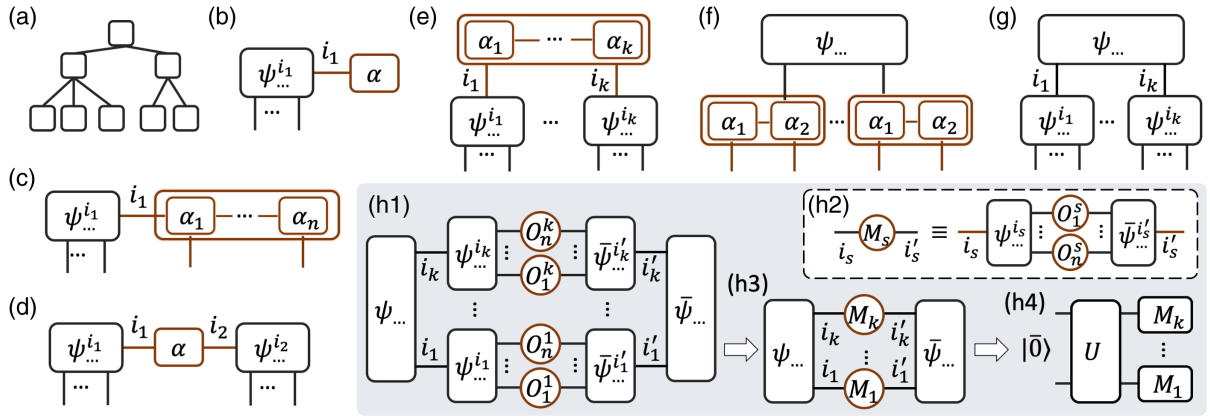

FIG. 2. Hybrid tree tensor networks. (a) An example tree structure. (b) Connection of a quantum tensor and a classical tensor. (c) Connection of a quantum tensor and a classical TN. (d) Connection of two quantum tensors via a classical tensor. (e) Generalization of (d) with multiple subsystems. (f) Using classical tensors to represent local correlation and a quantum tensor to represent correlations between subsystems. (g) A quantum-quantum network. (h1)–(h4) An example for calculating expectation values of (g). To calculate (h1) the expectation value of local observables $\otimes_{i=1}^{k}\otimes_{j=1}^{n} O_j^i$, we first calculate (h2) the observable $M_s^{i'_s,i_s}$ for each tensor on the second layer with quantum circuits shown in Figs. 1(e1) and 1(e2), which converts to the contraction in (h3) and the measurement using the quantum circuit (h4).

we can represent both of them with quantum states, as shown in Fig. 2(g), and expectation values of local observables can be efficiently obtained in Fig. 2(h).

Our results can be naturally generalized to an arbitrary tree structure. For a tree with maximal depth D, maximal degree g, and bond dimension κ, hybrid TTNs represent a system of $N = \mathcal{O}(g^{D-1})$ qubits. The number of circuits and the classical cost (using MPS) for measuring local observables scale as $\mathcal{O}(N\kappa^2)$ and $\mathcal{O}(Ng\kappa^4)$, respectively. We also show the contraction cost for trees with loops and its capability in representing entanglement beyond the area law in Ref. [21]. Since the hybrid TTN represents a large set of quantum states and admits efficient calculation of local observables, it can be used for variational quantum simulation for solving static and dynamic problems of large quantum systems.

Numerical simulation.—We test the effectiveness of hybrid TNs in finding ground states of 1D and 2D spin lattice systems with nearest-neighbor interactions and external fields in Fig. 3. For 1D spin clusters, we regard each adjacent $n = 8$ qubit as a subsystem and consider $k = 2, 3, \ldots, 8$ subsystems with $n \times k$ qubits. A general form of the Hamiltonian is $H = \sum_{j=1}^{k} H_j + \lambda H_{\text{int}}$, where $H_j = \sum_{i=1}^{7} f\hat{Z}_{8j+i}\hat{Z}_{8j+i+1} + \sum_{i=1}^{8}(g\hat{X}_{8j+i} + h\hat{Z}_{8j+i})$ and $H_{\text{int}} = \sum_{j=1}^{k-1} f_j\hat{Z}_{8j}\hat{Z}_{8j+1}$ represent the Hamiltonian of the jth subsystem and their interactions, respectively, with interaction strength λ. Here $\hat{X}_i$ and $\hat{Z}_i$ are Pauli operators acting on the ith qubit. For the 2D $n \times k$ spin lattice, we group each $n = 3 \times 3$ qubit on a small square lattice as a subsystem and consider $k = N_x \times N_y$ subsystems with N_x (N_y) subsystems along x (y) direction. The 2D Hamiltonian is $H = \sum_{\langle i,j\rangle} f_{ij}\hat{Z}_i\hat{Z}_j + \sum_i(g\hat{X}_i + h\hat{Z}_i)$, where $\langle i, j\rangle$ represents all the nearest-neighbor pairs on a square lattice. We consider that the interactions in each subsystem are identical $f = 1$, while interactions on the boundary of nearest-neighbor subsystem $\{f_j\}$ or $\{f_{i,j}\}$ are generated randomly from [0, 1], as shown in Fig. 3(a). The parameters of the external fields are set as $h = 1/\pi = 0.32$ and $g = 0.5$.

Considering the hybrid TTN of Fig. 2(g), the first layer state and the jth subsystem of the second layer are generated as $|\psi\rangle = V(\vec{\theta}_0)|\bar{0}^0\rangle = \sum \alpha_{i_1,\ldots,i_k}|i_1, \ldots, i_k\rangle$ and $|\psi_j^{i_j}(\vec{\theta}_j)\rangle = U(\vec{\theta}_j)|\bar{0}^{i_j}\rangle$, respectively, with V and U shown in Fig. 3(b) and initial states $|\bar{0}^{i_j}\rangle = |i_j\rangle^{\otimes n}$, $i_j \in \{0, 1\}$. The hybrid TTN represents a quantum state $|\tilde{\psi}(\vec{\theta})\rangle = \sum_{i_1\ldots i_k}\alpha_{i_1,\ldots,i_k}(\vec{\theta}_0)|\psi_1^{i_1}(\vec{\theta}_1)\rangle \otimes \cdots \otimes |\psi_k^{i_k}(\vec{\theta}_k)\rangle$, with $\vec{\theta} = (\vec{\theta}_0, \vec{\theta}_1, \ldots, \vec{\theta}_k)$ representing all the parameters. The state is automatically normalized since $\langle\psi_j^{i'_j}|\psi_j^{i_j}\rangle = \delta_{i'_j,i'_j}$. For parameters $\vec{\theta}$, we obtain the energy expectation value $E(\vec{\theta}) = \langle\tilde{\psi}(\vec{\theta})|H|\tilde{\psi}(\vec{\theta})\rangle$ by following the contraction rule of Fig. 2(h). We use variational imaginary time evolution to minimize the energy $E(\vec{\theta})$, which requires an ancillary qubit (see Refs. [21,36]). Thus the quantum systems needed for simulating the $8 \times k$-qubit 1D and $9 \times k$-qubit 2D systems need $8 + 1$ and $9 + 1$ qubits, respectively.

We benchmark the calculation by comparing with open-boundary MPS for 1D systems and imaginary time evolution PEPS for 2D systems. We consider the relative error $1 - E/E_0$ with the ground state energy E from hybrid TTN calculation, and E_0 from MPS or PEPS. In Figs. 3(c1) and 3(d1), we study the convergence of ground state energy of 1D [Fig. 3(c1)] and 2D [Fig. 3(d1)] systems with coupling strength $\lambda = 1$ on 8×8 and 9×4 qubits, respectively, and

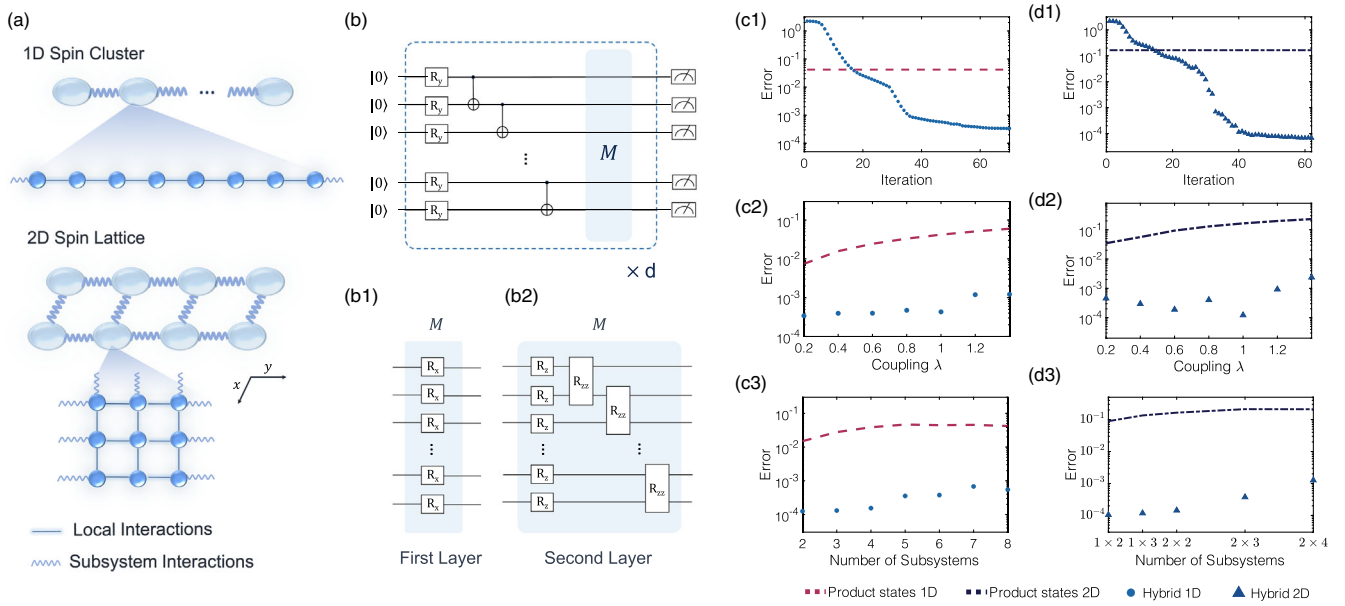

FIG. 3. Numerical simulation for 1D and 2D quantum systems with hybrid TTN. (a) 1D spin cluster and 2D spin lattice with interactions (thin lines) on the boundary. The interactions of subsystems are represented by thick lines. We group 8 adjacent qubits and 3×3 qubits on a square sublattice as subsystems for the 1D and 2D systems, respectively. (b) The ansatz circuit for the quantum tensors in Fig. 2(g). The circuits of both layers share similar structures with d repetitions of circuits in the dashed box. Here, R_α ($\alpha \in \{\hat{X}, \hat{Y}, \hat{Z}\}$) represents single-qubit rotation around α axis and the two-qubit gate is $R_{ZZ}(\theta_i) = e^{-i\theta_i \hat{Z}\otimes\hat{Z}}$. The rotation angle (parameter) for each gate is initialized from a small random value and updated in each variational cycle. The circuit depths for V (first layer tensor) and U (second layer tensor) are $d(V) = 6$ and $d(U) = 8$. The additional unitary M is inserted at the first and $[d/2 + 1]$th block of the first layer (b1) and the second layer (b2). (c),(d) Simulation results of the ground state energy. For the 1D and 2D cases, we compare E to the reference results $E_0 = E_{\mathrm{MPS}}$ and $E_0 = E_{\mathrm{PEPS}}$ obtained from a standard density matrix renormalization group with bond dimension $\kappa = 32$ and from PEPS imaginary time evolution with bond dimension $\kappa = 5$ and maximum allowed boundary bond dimension of $\tilde{\kappa} = 64$ during the contraction. We use the relative error $1 - E/E_0$ to characterize the accuracy. The red dashed line (1D) and blue dash-dotted line (2D) correspond to the energy using tensor products of the ground state of local subsystems. The cyan dot (1D) and blue triangle (2D) are results obtained with hybrid TNs. (c1),(d1) Convergence toward the ground state for the 1D 8×8 and 2D 9×4 systems with $\lambda = 1$, respectively. (c2),(d2) Error versus different subsystem coupling strength λ for the 1D 8×8 and 2D 9×4 systems, respectively. (c3), (d3) Errors with different numbers of local subsystems with $\lambda = 1$, respectively.

show a relative error below 10^{-3}. Next, we study how the coupling strength or the number of subsystems affect the efficacy of hybrid TTN. We present the calculation error with respect to different λ for the 8×8-qubit 1D and 9×4-qubit 2D systems in Figs. 3(c2) and 3(d2), respectively. We find that although the error fluctuates with different coupling strength, which might owe to instability from the optimization, the error remains consistent around 10^{-3}. In Figs. 3(c3) and 3(d3), we show the calculation error for the 1D with k subsystems [Fig. 3(c3)] and 2D with $N_x \times N_y$ subsystems [Fig. 3(d3)] for $\lambda = 1$, and we can achieve a desired simulation accuracy. These results with different coupling strength and number of subsystems verify the effectiveness and robustness of the hybrid TTN method. We refer to Ref. [21] for simulation details.

Applications.—While we are not expecting that the hybrid TN applies universally to arbitrary quantum systems in a similar way to universal quantum computers, we do anticipate hybrid TNs find their applications in a wide class of problems such as chemistry, many-body physics, quantum field theory, and quantum gravity [21]. Assisted by classical computers, hybrid TN could more efficiently represent multipartite quantum states and bolster the power of near-term quantum computers to significantly alleviate the limitations on the number of controllable qubits and circuit depth.

Ideas corresponding to simple hybrid TTNs of Figs. 2(b) and 2(c) have been studied for representing excited energy eigenstates [28] and active plus virtual orbitals [16] in electronic structure calculation. While the scheme in Ref. [16] assumed the configuration interaction ansatz for the virtual orbitals, a general classical TN may be used instead to improve the approximation (see Ref. [37]). Another application of the hybrid TN is to go beyond the Born-Oppenheimer approximation, which may have applications in understanding radiationless decay between electronic states [38], relativistic effects [39], or conical intersections [40–42]. Hybrid TNs could also be used for investigating the cluster systems [43,44], toy models for high energy physics [45–51], correlated

materials [31–33,52], as well as for exploring emergent quantum phenomena [53–56], including searching for Majorana zero modes and topological phase transitions [57–61]. We refer to Ref. [21] for detailed discussions.

Discussion.—We proposed a framework of hybrid tensor networks and studied its application in variational quantum simulation. Targeting practical problems that have both classical and genuine quantum effects, hybrid TNs integrate the power of classical TN theories and quantum computing, and hence enable quantum simulation of large-scale problems with small quantum processors and shallower circuits. Our work is different from proposals of using a quantum computer to contract a classical TN [62–65], whose generalization to hybrid TN could be a further work. Besides TNs, there also exist other powerful classical methods, such as quantum Monte Carlo [66,67] and machine learning with neural networks [68,69]. A future direction is to investigate the combination of these methods with quantum computing. Another independent approach of simulating large quantum systems with small quantum computers is to decompose multiqubit gates into a mixture of single-qubit gates [70–74], whose combination with our method may lead to an interesting future direction. After showing advantages over classical supercomputers in certain tasks [75,76], the next milestone is to solve practically meaningful and classically intractable tasks. Our work sheds light on the avenue for achieving this goal with near-term hardware.

We thank Suguru Endo, Patrick Hayden, Arthur Jaffe, Sam McArdle, John Preskill, Vlatko Vedral, and Ying Li for insightful, related discussions and comments. J. S. thanks Chenbing Wang for useful discussions on the numerics. X. Y acknowledges support from the Simons Foundation. J. L. is supported in part by the Institute for Quantum Information and Matter (IQIM), an NSF Physics Frontiers Center (NSF Grant No. PHY-1125565) with support from the Gordon and Betty Moore Foundation (GBMF-2644), and by the Walter Burke Institute for Theoretical Physics. Q. Z. acknowledges the support by the U.S. Department of Defense through the Hartree Postdoctoral Fellowship at QuICS. Y. Z. was supported in part by the Templeton Religion Trust under Grant No. TRT 0159 and by the ARO under Contract No. W911NF1910302.

Note added.—Recently, a relevant work was posted by Fujii *et al.* [77]. They suggest a divide-and-conquer method for solving a larger problem with smaller size quantum computers in a similar vein to Fig. 2(g) (see Ref. [21] for details). While their work used a different language and focused on different examples, our results are consistent and can be compared.

*xiaoyuan@pku.edu.cn
†jinzhao.sun@physics.ox.ac.uk
‡jliu2@caltech.edu
§zhaoq@umd.edu
‖you_zhou@g.harvard.edu

[1] S. R. White, Phys. Rev. Lett. **69**, 2863 (1992).
[2] S. Rommer and S. Östlund, Phys. Rev. B **55**, 2164 (1997).
[3] R. Orús, Nat. Rev. Phys. **1**, 538 (2019).
[4] R. P. Feynman, Int. J. Theor. Phys. **21**, 467 (1982).
[5] S. McArdle, S. Endo, A. Aspuru-Guzik, S. C. Benjamin, and X. Yuan, Rev. Mod. Phys. **92**, 015003 (2020).
[6] Y. Cao, J. Romero, J. P. Olson, M. Degroote, P. D. Johnson, M. Kieferová, I. D. Kivlichan, T. Menke, B. Peropadre, N. P. Sawaya *et al.*, Chem. Rev. **119**, 10856 (2019).
[7] J. O'Gorman and E. T. Campbell, Phys. Rev. A **95**, 032338 (2017).
[8] Near-term quantum devices refers to quantum hardware processing tens to hundreds of qubits with relatively noisy operations. These types of devices are in hand now and will be greatly improved in the near future, although they are yet insufficient to realize universal quantum computing. A potential use of near-term quantum devices is to demonstrate quantum advantage and develop specific applications, such as quantum chemistry and materials.
[9] J. Preskill, Quantum **2**, 79 (2018).
[10] E. Altman, K. R. Brown, G. Carleo, L. D. Carr, E. Demler, C. Chin, B. DeMarco, S. E. Economou, M. A. Eriksson, K.-M. C. Fu *et al.*, PRX Quantum **2**, 017003 (2021).
[11] S. Wang, E. Fontana, M. Cerezo, K. Sharma, A. Sone, L. Cincio, and P. J. Coles, arXiv:2007.14384.
[12] M. Cerezo and P. J. Coles, Quantum Sci. Technol. **6**, 035006 (2021).
[13] S. Endo, Z. Cai, S. C. Benjamin, and X. Yuan, J. Phys. Soc. Jpn. **90**, 032001 (2021).
[14] M. Cerezo, A. Arrasmith, R. Babbush, S. C. Benjamin, S. Endo, K. Fujii, J. R. McClean, K. Mitarai, X. Yuan, L. Cincio, and P. J. Coles, arXiv:2012.09265.
[15] K. Bharti, A. Cervera-Lierta, T. H. Kyaw, T. Haug, S. Alperin-Lea, A. Anand, M. Degroote, H. Heimonen, J. S. Kottmann, T. Menke, W.-K. Mok, S. Sim, L.-C. Kwek, and A. Aspuru-Guzik, arXiv:2101.08448.
[16] T. Takeshita, N. C. Rubin, Z. Jiang, E. Lee, R. Babbush, and J. R. McClean, Phys. Rev. X **10**, 011004 (2020).
[17] F. Barratt, J. Dborin, M. Bal, V. Stojevic, F. Pollmann, and A. G. Green, npj Quantum Inf. **7**, 79 (2021).
[18] X. Yuan, S. Endo, Q. Zhao, Y. Li, and S. C. Benjamin, Quantum **3**, 191 (2019).
[19] L. Hackl, T. Guaita, T. Shi, J. Haegeman, E. Demler, and I. Cirac, SciPost Phys. **9**, 048 (2020).
[20] U. Schollwöck, Ann. Phys. (Amsterdam) **326**, 96 (2011).
[21] See Supplemental Material at http://link.aps.org/supplemental/10.1103/PhysRevLett.127.040501 for the framework of hybrid tensor networks, implementations, examples of tree structures, and potential applications in detail.
[22] M. Fannes, B. Nachtergaele, and R. F. Werner, Commun. Math. Phys. **144**, 443 (1992).
[23] A. Klumper, A. Schadschneider, and J. Zittartz, J. Phys. A **24**, L955 (1991).
[24] A. Klümper, A. Schadschneider, and J. Zittartz, Europhys. Lett. **24**, 293 (1993).
[25] F. Verstraete and J. I. Cirac, arXiv:cond-mat/0407066.

[26] Y.-Y. Shi, L.-M. Duan, and G. Vidal, Phys. Rev. A **74**, 022320 (2006).
[27] G. Vidal, Phys. Rev. Lett. **99**, 220405 (2007).
[28] J. R. McClean, M. E. Kimchi-Schwartz, J. Carter, and W. A. de Jong, Phys. Rev. A **95**, 042308 (2017).
[29] J. I. Colless, V. V. Ramasesh, D. Dahlen, M. S. Blok, M. E. Kimchi-Schwartz, J. R. McClean, J. Carter, W. A. de Jong, and I. Siddiqi, Phys. Rev. X **8**, 011021 (2018).
[30] J. R. McClean, Z. Jiang, N. C. Rubin, R. Babbush, and H. Neven, Nat. Commun. **11**, 636 (2020).
[31] S. Wouters, C. A. Jiménez-Hoyos, Q. Sun, and G. K.-L. Chan, J. Chem. Theory Comput. **12**, 2706 (2016).
[32] N. Lanata, Y. Yao, C.-Z. Wang, K.-M. Ho, and G. Kotliar, Phys. Rev. X **5**, 011008 (2015).
[33] G. Rohringer, H. Hafermann, A. Toschi, A. A. Katanin, A. E. Antipov, M. I. Katsnelson, A. I. Lichtenstein, A. N. Rubtsov, and K. Held, Rev. Mod. Phys. **90**, 025003 (2018).
[34] X. Chen, Z.-C. Gu, and X.-G. Wen, Phys. Rev. B **82**, 155138 (2010).
[35] X. Chen, Z.-C. Gu, and X.-G. Wen, Phys. Rev. B **83**, 035107 (2011).
[36] S. McArdle, T. Jones, S. Endo, Y. Li, S. C. Benjamin, and X. Yuan, npj Quantum Inf. **5**, 75 (2019).
[37] S. Szalay, M. Pfeffer, V. Murg, G. Barcza, F. Verstraete, R. Schneider, and Ö. Legeza, Int. J. Quantum Chem. **115**, 1342 (2015).
[38] G. A. Worth and L. S. Cederbaum, Annu. Rev. Phys. Chem. **55**, 127 (2004).
[39] M. Reiher and A. Wolf, *Relativistic Quantum Chemistry: The Fundamental Theory of Molecular Science* (John Wiley & Sons, New York, 2014).
[40] W. Domcke, D. R. Yarkony, and H. Köppel, *Conical Intersections* (World Scientific, Singapore, 2004).
[41] W. Domcke and D. R. Yarkony, Annu. Rev. Phys. Chem. **63**, 325 (2012).
[42] I. G. Ryabinkin, L. Joubert-Doriol, and A. F. Izmaylov, Acc. Chem. Res. **50**, 1785 (2017).
[43] E. Garlatti, T. Guidi, S. Ansbro, P. Santini, G. Amoretti, J. Ollivier, H. Mutka, G. Timco, I. Vitorica-Yrezabal, G. Whitehead *et al.*, Nat. Commun. **8**, 14543 (2017).
[44] G. A. Timco, S. Carretta, F. Troiani, F. Tuna, R. J. Pritchard, C. A. Muryn, E. J. McInnes, A. Ghirri, A. Candini, P. Santini *et al.*, Nat. Nanotechnol. **4**, 173 (2009).
[45] Y. Gu, X.-L. Qi, and D. Stanford, J. High Energy Phys. 05 (2017) 125.
[46] P. Hayden and J. Preskill, J. High Energy Phys. 09 (2007) 120.
[47] J. Maldacena, D. Stanford, and Z. Yang, Fortschr. Phys. **65**, 1700034 (2017).
[48] J. Maldacena and X.-L. Qi, arXiv:1804.00491.
[49] B. Yoshida and A. Kitaev, arXiv:1710.03363.
[50] J. Maldacena and D. Stanford, Phys. Rev. D **94**, 106002 (2016).
[51] J. M. Maldacena, Int. J. Theor. Phys. **38**, 1113 (1999).
[52] H. Ma, M. Govoni, and G. Galli, npj Comput. Mater. **6**, 1 (2020).
[53] Y. Zhou, K. Kanoda, and T.-K. Ng, Rev. Mod. Phys. **89**, 025003 (2017).
[54] F. Liu, R. Lundgren, P. Titum, G. Pagano, J. Zhang, C. Monroe, and A. V. Gorshkov, Phys. Rev. Lett. **122**, 150601 (2019).
[55] M. Sato and Y. Ando, Rep. Prog. Phys. **80**, 076501 (2017).
[56] A. V. Chubukov, D. V. Efremov, and I. Eremin, Phys. Rev. B **78**, 134512 (2008).
[57] R. t. Lutchyn, E. Bakkers, L. P. Kouwenhoven, P. Krogstrup, C. Marcus, and Y. Oreg, Nat. Rev. Mater. **3**, 52 (2018).
[58] Y. You, T. Devakul, F. J. Burnell, and S. L. Sondhi, Phys. Rev. B **98**, 035112 (2018).
[59] J. Alicea, Rep. Prog. Phys. **75**, 076501 (2012).
[60] J. D. Sau, S. Tewari, R. Lutchyn, T. Stanescu, and S. Das Sarma, Phys. Rev. B **82**, 214509 (2010).
[61] C. Beenakker, Annu. Rev. Condens. Matter Phys. **4**, 113 (2013).
[62] I. H. Kim and B. Swingle, arXiv:1711.07500.
[63] I. H. Kim, arXiv:1703.00032.
[64] I. H. Kim, arXiv:1702.02093.
[65] J.-G. Liu, Y.-H. Zhang, Y. Wan, and L. Wang, Phys. Rev. Research **1**, 023025 (2019).
[66] W. M. C. Foulkes, L. Mitas, R. J. Needs, and G. Rajagopal, Rev. Mod. Phys. **73**, 33 (2001).
[67] J. Carlson, S. Gandolfi, F. Pederiva, S. C. Pieper, R. Schiavilla, K. E. Schmidt, and R. B. Wiringa, Rev. Mod. Phys. **87**, 1067 (2015).
[68] G. Carleo and M. Troyer, Science **355**, 602 (2017).
[69] Y. Li, arXiv:1701.07274.
[70] T. Peng, A. W. Harrow, M. Ozols, and X. Wu, Phys. Rev. Lett. **125**, 150504 (2020).
[71] S. Bravyi, G. Smith, and J. A. Smolin, Phys. Rev. X **6**, 021043 (2016).
[72] J. Sun, S. Endo, H. Lin, P. Hayden, V. Vedral, and X. Yuan, arXiv:2106.05938.
[73] K. Mitarai and K. Fujii, arXiv:1909.07534.
[74] K. Mitarai and K. Fujii, Quantum **5**, 388 (2021).
[75] F. Arute, K. Arya, R. Babbush, D. Bacon, J. C. Bardin, R. Barends, R. Biswas, S. Boixo, F. G. Brandao, D. A. Buell *et al.*, Nature (London) **574**, 505 (2019).
[76] C. Huang, F. Zhang, M. Newman, J. Cai, X. Gao, Z. Tian, J. Wu, H. Xu, H. Yu, B. Yuan, M. Szegedy, Y. Shi, and J. Chen, arXiv:2005.06787.
[77] K. Fujii, K. Mitarai, W. Mizukami, and Y. O. Nakagawa, arXiv:2007.10917.